RSC Advances

ROYAL SOCIETY OF CHEMISTRY

www.rsc.org/advances

Vacuum-assisted layer-by-layer electrospun membrances: antibacterial and antioxidative applications

Bin Zhou[a,b], Xing Jin[c], Jing Li [a,b], Wei Xu[a,b], Shilin Liu[a,b], Yan Li [a,b], Bin Li* [a,b]

[a] College of Food Science and technology, Huazhong Agriculture University, Wuhan 430070, China

[b] Key Laboratory of Environment Correlative Dietology (Huazhong Agricultural University), Ministry of Education

[c] Department of Clinical Laboratory, Xi'an Gaoxin Hospital, Xi'an 710075,China

* Corresponding author: Bin Li Tel.: +86 27 6373 0040 Fax: +86 27 8728 8636 E-mail: libinfood@mail.hzau.edu.cn

Abstract: Layer-by-layer assembled films have been exploited for functional materials. Tannic acid with previously confirmed antibacterial and antioxidant potential was deposited on cellulose nanofibrous mats. LbL assembly technique allowed sufficient binding of TA and AgNPs-Lys to the supporting substrate via hydrogen bond and electrostatic interaction. The properties and morphology of the AgNPs-Lys/TA multilayer assembly membrances were characterized by X-ray photoelectron spectroscopy (XPS), Fourier transform infrared spectra (FT-IR), wide-angle X-ray diffraction (XRD), and scanning electron microscopy (SEM). The antibacterial and antioxidant activities were examined as well. The hybrid composite films have potential application in food packing and wound dressing, and tissue engineering, etc.

Keywords: Silver nanoparticles, Tannic acid, Antibacterial, Antioxidant, Electrospinning, Layer-by-layer

1. Introduction

During the last years，materials based on one-dimensional nanostructures, such as nanofibers, nanotubes, nanowires, have created a subject of substantial interest due to their unique properties [1, 2]. And electrospinning is efficient and straightforward method of producting ultrafine fibers with micro- to nano-meter range diameters and with controlled surface morphology [3, 4]. Because of their high specific surface area, high porosity, small pore size and 3D structure, the nanofibrous materials may find diverse applications, for example, from electronics and military clothing to cosmetics, pharmacy and medicine [5-7].

In order to develop electrospun nanofibers as useful nanobiomaterials, surface of them have been functionalized by various surface modification technique [8], such as surface graft polymerization [9, 10], co-electrospinning [11], plasma treatment [12], wet chemical method [13]. A versatile surface modification method that allows surface coating with thickness from a few nano to several micrometers through precise control has been realized by layer-by-layer (LbL) polyelectrolyte multilayer assembly [14,15].

Layer-by-layer multilayer membrane fabrication is an attractive fabrication strategy because of the large variety of charged polymers that can be utilized in LbL assembly. Additionally, the membrane structure can be readily tailored by altering the polymer deposition conditions. This technique has been widely used to fabricate thin films from polymer pairs with complementary functional groups because of its advantages over other methods [16].

Lysozyme (Lys) is a ubiquitous antibacterial enzyme against many food spoilage and pathogenic microorganisms by damaging the cell walls of bacteria [17, 18]. It consists of 129 amino acid residues with free carboxylic groups, amino groups and four disulfide bonds, and has been used to prepare Au nanoparticles (AuNPs), Ag nanoparticles (AgNPs), Au nanoclusters (AuNCs) and Ag nanoclusters (AgNCs) [19-21]. The AuNCs-Lys can target notorious pathogenic bacteria, including *E. coli* and *S. aureus* [22]. Moreover, tannic acid (TA) is a glucoside of gallic acid polymer with multiple phenolic hydroxyl groups that is found in many plants [23]. It is an attractive molecule known to have antitumor, antibacterial, and antioxidant activity [16], as well as reported interactions with proteins [24]. Because of the high pKa value of TA of ca. 8.5, its association through hydrogen bonding is expected to occur at neutral pH values [25]. So it has recently been incorporated in hydrogen-bonded LbL films at physiologic pH [24].

In the current study, the LbL films were fabricated from TA and AgNPs-Lys. LbL assembly technique allowed sufficient binding of TA and AgNPs-Lys to the supporting substrate via hydrogen bond and electrostatic interaction. The properties and morphology of the TA/AgNPs-Lys multilayer assembly membrances were characterized and the antibacterial and antioxidant activities were examined. The hybrid composite films have potential application in food packing and wound dressing.

Experimental

Chemicals and materials

Cellulose acetate (CA, *Mn* 30,000) was purchased from Sigma–Aldrich Co., USA. Hen egg white lysozyme and tannic acid were all obtained from Sinopharm Chemical Reagents Co., Ltd. (Shanghai, China). The other reagents were analytical grade purchased from China National Pharmaceutical Group Industry Corporation Ltd.. All aqueous solutions were prepared using purified water with a resistance of 18.2 MΩcm. *Escherichia.coli (E.coli)* and *Staphylococcus aureus (S.aureus)* were obtained from China Center for Type Culture 140 Collection, Wuhan University (Wuhan, China).

Synthesis of AgNPs-Lys

AgNPs-Lys were prepared using a procedure modified from that used by Mathew et al and Zhou [19, 26]. In a typical synthesis, 1 mL of 10 mM silver nitrate solution was added to 75 mg Lys powder in 5 mL distilled water solution with vigorous stirring at room temperature. The mixture solution was left to incubate for 5 minutes under vigorous stirring. Then about 0.3mL NaOH solution (1 M) was added followed by 0.48 mL $NaBH_4$ solution (10 mM) drop-wise until the solution turns from colorless to reddish brown, indicating the formation of silver nanoparticles. The product of different stages were characterized by ultraviolet-visible spectrum (UV-vis) and FT-IR. The hydrodynamic diameter measured using dynamic light scattering (DLS).

Fabrication of template nanofibers

The CA electrospun nanofibrous membranes were fabricated using a set of homemade electrospinning setup, which contained a high voltage supply (DW-P303-1ACD8, Tianjin Dongwen Co., China), a syringe pump (LSP02-1B, Baoding Longer Precision Pump Co., Ltd., China) and a grounded rotary collector. Nanofibrous CA mats were

fabricated by modified Ding's method [27]. 2 g CA was dissolved into 8 g acetone/N, N-dimethyl acetamide (DMAc) (2:1, W/W) mixed solvent and stirred to obtain homogeneous solution. Then it was loaded into a plastic syringe, which was driven by a syringe pump. The applied voltage was 16 kV and the tip-to-collector distance was 20 cm. The ambient temperature and relative humidity were maintained at 25℃ and 45%, respectively. The prepared fibrous mats were dried at 80℃ in vacuum for 24 h to remove the trace solvent. Hydrolysis of the CA mats was performed in alkaline aqueous solution at ambient temperature for 7 days following the previous report [28].

Formation of nanocomposite films on template nanofibers

The bilayer film was then deposited, by adding AgNPs@ Lys (1 mg/mL lysozyme, pH 7.4, in 0.01 M PBS) followed by tannic acid (1 mg/mL, pH 7.4, in 0.01 M PBS) each for 50mL. Then, the solution was suction-filtered through the nanofibrous mats. Following each deposition step, the mats wash with 50 mL 0.01 M PBS (pH 7.4) [24, 29]. The water was suction-filtered through the nanofibrous mats as well. Here, $(AgNPs\text{-}Lys/TA)_n$ was used as a formula to label the LbL structured films, where n was the number of the AgNPs-Lys/TA bilayers. The outermost layer was Lys composite when n equaled to 5.5 and 10.5. The LbL films coated fibrous mats were dried at 40 ℃ for 2 h under vacuum prior to further characterizations.

Characterization

The morphology characterization of the composite membrances was performed using scanning electron microscopy (SEM) (S-4800, Hitachi Ltd., Japan). The dismeters of the fibers were measured using Nano measure 1.2.5. Fourier transform infrared

(FT-IR) spectra were acquired on a Nicolet170-SX instrument (Thermo Nicolet Ltd., USA) in the wavenumber range of 4000-400 cm^{-1}. X-ray photoelectron spectroscopy (XPS) was conducted on an axis ultra DLD apparatus (Kratos, U.K.). X-ray diffraction (XRD) was carried out using a diffract meter type D/max-rA (Rigaku Co., Japan) with Cu target and Ka radiation (λ= 0.154 nm).

In vitro antibacterial activity assay

The inhibition zone test was used to study the bacterial inhibition activity of nanofibrous mats. Gram-negative *E. coli* and gram-positive *S. aureus* were selected as representative microorganism and cultivated in culture medium in an incubator. Unmodified cellulose mats were used as negative control. The testing mats were cut into round disks with a diameter of 6 mm, sterilized under an ultraviolet radiation lamp for 30 min. One hundred micro-liters of 5.0-10.0×10^5 cfu/mL *E. coli* or 5.0-10.0×10^5 cfu/mL *S. aureus* bacteria levitation liquid was placed onto pre-autoclave sterilized meat-peptone broth and coated uniformly, respectively. Then the prepared mats were tiled on the surface of meat-peptone broth to cling to the bacteria levitation liquid. After incubated at 37 ℃ in an air-bathing thermostat shaker with a rotating speed of 120 r/min for 24h, the bacteria inhibition zones were measured by a micrometer with a tolerance of one millimeter. All of the experiments were conducted in triplicate with data reported as mean ± standard deviation.

In vitro antioxidant activity assay

The antioxidant activity of nanocomposite films were measured according to the DPPH method with minor modification [30, 31]. Briefly, scavenging activity assay

was carried out by recording the absorbance of DPPH solution (100 μM) at 517 nm in the presence of the nanofibrous mats above at room temperature with a UV-vis spectrophotometer. The free radical scavenging potency of the nanofirous mats were expressed as the percentage of DPPH that was decreased in comparison with that of the control condition after 30 min preservation in the dark.

Results and discussion

Preparation and characterization of AgNPs-Lys

The as-prepared AgNPs-Lys was characterized by UV–visible absorption as indicated in Fig. 1A. It can be observed that the UV–visible absorption spectrum of AgNPs-Lys exhibited a peak at 420 nm due to surface plasmon resonance of Ag nanoparticles. And the hydrodynamic diameter of AgNPs-Lys measured using DLS was 6.76±0.44nm. In addition, the surface chemistry of AgNPs-Lys was evaluated using FT-IR. The FT-IR spectra as shown in Fig. 1B showed that there was no S–H stretching band for Lys only contains four disulfide bonds without a free hydrosulfide group. However, an S–H stretching band around 2485 cm^{-1} appeared after the natural Lys was incubated in a solution of pH about 12, as the alkali could cleave the disulfide bonds of Lys [19]. The peak at 2485 cm^{-1} almost disappeared after the formation of AgNPs-Lys, indicating that Lys was modified on the surface of AgNPs through Ag–S interactions.

Surface morphology analysis AgNPs-Lys/TA nanofibrous membrances

In order to investigate the effect of AgNPs-Lys and TA deposition on the morphology of the cellulose nanofibous mats, the SEM images of the composite fibrous mats were

177 taken. The representative scanning electron microscopy (SEM) image of nanofibrous
178 mats shown in Fig. 2a revealed randomly oriented 3D nonwoven membranes with an
179 average diameter of 600 nm. And the cellulose nanofibers exhibited cylindrical shape
180 and was continuous and long without any defects (Fig. 2a and a'). To study the impact
181 of the number of coating bilayers on the formation of composite films, the cellulose
182 fibers were coated with various bilayers of AgNPs-Lys and TA.
183 Not only the diameter but also the morphology of all composite mats changed
184 obviously caused by the deposited of AgNPs-Lys and TA on the surface of nanofibers.
185 After LbL coating process, the nanofibers showed a much higher surface roughness
186 on each fiber compared with the smooth surface of the cellulose (Fig. 2a-e, a'-e').
187 There are many granules on the surface of the fibers, which was attributed to the
188 interaction between Lys and TA. Moreover, with the increase of the bilayer number,
189 some junctions among the cellulose fibers can be seen, which caused by the
190 aggregation of AgNPs-Lys and TA. As displayed in Fig. 2d', we can see that after the
191 coating, a AgNPs-Lys/TA shell layer was visible around the cellulose nanofibers.
192 These images visually confirmed that AgNPs-Lys and TA were successfully
193 assembled onto the surface of the fibers.

194 **Surface composition analysis of AgNP-Lys/TA nanofirous mats**

195 To further comfirm the depositon of AgNP@Lys and TA on the LbL films, XPS scan
196 were performed to verify the surface chemical composition of the composite
197 nanofibrous mats. Fig. 3A displays the survey scan spectrum of AgNPs-Lys/TA
198 composite mat, in which C 1s, O 1s, N 1s, S 2p, and Ag 3d core-levels exist obviously.

As sown in Figure 3B, the C 1s core-level photoelectron spectrum can be curved into three peak components located at 284.6 eV, 286.0 eV, and 288.2 eV, which are assigned to C-C, C-O, and C=O or O-C=O group from TA or Lys [32]. Moreover, the N 1s spectrum had one peak centered at 399.8 eV which was characteristic of pyridinic nitrogen (sp^2 hybrization), and it was associated with the assignment of the binding energy of C-N covalent bonds [33]. As all of cellulose, Lys and TA contained C and O, the presence of them cannot certify that TA was deposited on the surface of the fibers successfully. To further demonstrate LbL coating process in every layer, the ratio of C/O was measured (Table 1). As is well-known, TA was rich in oxygen, 43.27%, much higher than in Lys. From the obtained atomic concentration of the high resolution scans (C 1s and O 1s), the C/O ratio of $(AgNP@Lys/TA)_{10}$ and $(AgNP@Lys/TA)_{10.5}$ were obtained to be 2.22 and 3.02, respectively. In addition, the S 2p signal at *ca.* 163 eV (Fig. 3E) implied the presence of sulfur species on the surface of composite nanofibers. As shown in Fig. 2F, two peaks at 368.2 eV and 374.2 eV were observed in the Ag 3d XPS spectra of $(AgNP@Lys/TA)_{10}$ and $(AgNP@Lys/TA)_{10.5}$ nanofibrous mats corresponding to Ag $3d_{5/2}$ and Ag $3d_{3/2}$, respectively. These results are in good agreement with the results of Zhou et al. [19]. The presence of signal at 368.2 eV revealed that Ag^+ exist in the complex [34]. The Moreover, with the increase of particle size, the binding energy would have a slight blue shift to about 367.7 eV [34]. For the core-level spectra of $(AgNP@Lys/TA)_{10}$ and $(AgNP@Lys/TA)_{10.5}$, the intensity of the peaks have significant difference, which was attributed to the difference of elemental composition.

FT-IR spectra of AgNPs-Lys/TA nanofibrous mats

The successful assembly of the AgNPs-Lys and TA to cellulose nanofibers can also be illustrated by the FT-IR spetra. As shown in Figure 4, the abroad band in the region of about 3500~3100 cm^{-1} was attributed to the free O-H stretching vibration of hydroxyl groups in cellulose molecules (Fig. 4g) [35]. The absorption bands at 2898 cm^{-1} was assigned to the C-H stretching. The emergence of a peak at 1637cm^{-1} corresponding to –OH bending of the nanofibrous mats [36]. The bond at 1066cm^{-1} was assigned to the sretching of C-O, asymmetric stretching of C-O-C bond of the glycosidic linkage and pyranose ring of cellulose were observed at around 1238, 1164 and 1052cm^{-1}, respectively. And the 897cm^{-1} was attributed to the C_1-H deformation vibrations of cellulose [37]. The two common bands of amino group observed at 1654 cm^{-1} and 1540 cm^{-1} belongs to the amide I and amide II peaks, which confirmed that Lys was assembly on the surface of cellulose films successfully (Fig. 4a, c-f). For the composite nanofibrous mats, the observed increase in intensity of the peak positioned at 1716 cm^{-1} as a shoulder of the amide I or –OH bending can be due to the carbonyl CO vibration of the TA ester bond (Fig. 4c-f). The 1616 cm^{-1} and 1533 cm^{-1} are attributed to C=C stretching vibrations of aromatic ring and carbon chain, respectively. The peak at 1448 cm^{-1} is associated with C-O-H in plane bend of hydroxyl group in TA. The band at 1323 cm^{-1} and 1203 cm^{-1} can be attributed to C-O stretch of the acid group in TA and C-O stretch in polyols, respectively (Fig. 4b) [38]. The absorbtion band centered at 1032 cm^{-1} is associated with the C-O-C bending mode [39]. The weak absorbtion band at 876 cm^{-1} is assigned to O-H out of plane bending mode of

the acid group. The band at 758 cm^{-1} can be related to the C-H out plane bend of phenyl group (Fig. 4b) [39].

Crystalline property of AgNPs-Lys/TA nanofibrous mats

The XRD patterns of samples are presented in Figure 5. From Figure 5a, we can see a broad peak ranged from about 15° to 32° corresponding to amorphous region of TA. The diffractogram of cellulose nanofibers consisted of a peak at 12.2, 20.1, and 21.8° corresponding to typical cellulose crystal. After the coating, the peak at 21.8° corresponding to cellulose crystal increased in both Lys/TA and AgNPs-Lys/TA nanofibrous mats, which can be attributed to the deposition of TA. In addition, $(AgNPs\text{-}Lys/TA)_{10.5}$ had a well defined characteristic diffraction peak at 38.5° corresponding to (111) plane of face centered cubic crystal structure of silver revealing the presence of silver nanoparticles [40].

Free radical scavenging activity of AgNPs-Lys/TA nanofibrous mats using DPPH

Radical scavenging activities are very important due to the deleterious role of free radicals in foods and in biological systems [41]. To confirm the bioactivity, the DPPH scavenging assay was employed to determine the radical-scavenging ability of LbL coating nanofibours mats (Fig. 6). The method can evaluate the antiradical power of an antioxidant by measuring of a decrease in the absorbance of $DPPH^{\cdot}$ at 517 nm, which was accompanied by a colour change from purple to yellow. The deposition of AgNPs-Lys and TA on the fibers enhanced the antioxidant activity of composite nanofibrous mats compared to the cellulose nanofibrous mats. The antioxidant capacity of these membrances increased with the increase of the number of bilayer.

The scavenging rate of $(AgNPs\text{-}Lys/TA)_5$ and $(AgNPs\text{-}Lys/TA)_{10}$ were 70% and 82%, respectively. However, the antioxidant capacity decreased dramatically compared to $(AgNPs\text{-}Lys/TA)_5$ and $(AgNPs\text{-}Lys/TA)_{10}$ when the outmost component was AgNPs-Lys ($(AgNPs\text{-}Lys/TA)_{5.5}$ and $(AgNPs\text{-}Lys/TA)_{10.5}$). Since the presence of AgNPs-Lys on the outmos layer has a certain stereo-hindrance effect caused the decrease of the antioxidant capacity. We also investigated the relationship between scavenging rate and reaction time. The ratio of C_t to C_0 were obtained from the relative intensity ratios of the respective absorbance (A_t/A_0) at 517 nm. The rate constants *k* estimated directly from the slopes were $0.107min^{-1}$, $0.044min^{-1}$, $0.244min^{-1}$, and $0.094min^{-1}$ for $(AgNPs\text{-}Lys/TA)_5$, $(AgNPs\text{-}Lys/TA)_{5.5}$, $(AgNPs\text{-}Lys/TA)_{10}$, $(AgNPs\text{-}Lys/TA)_{10.5}$, respectively (Fig. 6B). The result was consistent with the result in Fig. 6A. As can be seen, the composite nanofibrous mats exhibited a good antioxidant performance.

Antibacterial property of AgNPs-Lys/TA nanofibrous mats

Both Lys and TA are ubiquitous antibacterial agent against many food spoilage and pathogenic microorganisms [8, 42]. We further examined the antibacterial activity of the cellulose nanofibrous mats and LbL coating mats against the Gram-negative bacteria (*E. coli*) and the Gram-positive bacteria (*S. aureus*). The antibacterial bioactivity of cellulse nanofibers and composite nanofibers with different bilayer numbers was also evaluated for comparison (Fig. 7). Obviously, as-prepared cellulose mats hardly displayed bacterial inhibition zones at all the studied time points. In contrast, an obvious bacterial inhibition zones on the composite nanofibrous mats can

be seen. For *S. aureus*, the antibacterial effect enhanced with the increase of the number of bilayer, which due to the fact that both TA and Lys have good antibacterial activity against *S. aureus*. However, Lys has a relatively weak antibacterial activity for Gram-negative bacillus because of the protection of lipopolysaccharide layer surrounding their outmost membrance [8]. So the composite nanofibrous mats with AgNPs-Lys on the outmost layer exhibit weaker antibacterial effect against *E. coli*.

Conclusions

AgNPs-Lys/TA multilayer nanofibrous mats were fabricated using electrospinning and electrostatic LbL assembly technique. The films were formulated based on interactions between Lys and TA at physiologic pH. The deposition of AgNPs-Lys and TA on the surface of cellulose mats was characterized by XPS, XRD, and FT-IR. Compared with the smooth surface of the cellulose, the morphology of composite nanofibrous mats became highly rough with increasing deposition layer. Moreover, all the composite nanofibrous mats examined were found to possess good DPPH-scavenging acitivity. Besides, the microbial inhibition assay demonstrated that the AgNPs-Lys/TA composite mats had good antibacterial effects. The antioxidant activity and antibacterials activity of the composite nanofibrous mats endows the materials with great potential application in the areas of food packing, tissue engineering, wound dressing, etc.

Acknowledgments

This work was financially supported by the National Natural Science Foundation of China (Grant No. 31371841). The authors greatly thank colleagues of Key Laboratory

of Environment Correlative Dietology of Huazhong Agricultural University for offering many conveniences.

Reference

1. B. Sun, Y. Z. Long, H. D. Zhang, M. M. Li, J. L. Duvail, X. Y. Jiang and H. L. Yin, *Prog. Polym. Sci.*, 2014, **39**, 862-890.
2. X. Wang, B. Ding, G. Sun, M. Wang and J. Yu, *Prog. Mater. Sci.*, 2013, **58**, 1173-1243.
3. X. Hu, S. Liu, G. Zhou, Y. Huang, Z. Xie and X. Jing, *J Control Release*, 2014, **185C**, 12-21.
4. J. Du, X. Li, C. Yang, W. Li, W. Huang, R. Huang, X. Zhou and H. Deng, *Current Nanoscience*, 2013, **9**, 8-13.
5. M. Ignatova, I. Rashkov and N. Manolova, Expert Opin Drug Deliv, 2013, **10**, 469-483.
6. S. Xin, X. Li, Q. Wang, R. Huang, X. Xu, Z. Lei and H. Deng, *J biomed. Nanotech.*, 2014, **10**, 803-810.
7. R. Huang, H. Deng, T. Cai, Y. Zhan, X. Wang, X. Chen, A. Ji and X. Li, *J biomed. Nanotech.*, 2014, **10**, 1346-1358.
8. B. Zhou, Y. Li, H. Deng, Y. Hu and B. Li, *Colloids Surf. B Biointerfaces*, 2014, **116C**, 432-438.
9. X. Tang, Y. Si, J. Ge, B. Ding, L. Liu, G. Zheng, W. Luo and J. Yu, Nanoscale, 2013, **5**, 11657-11664.
10. Y. Shang, Y. Si, A. Raza, L. Yang, X. Mao, B. Ding and J. Yu, Nanoscale, 2012, **4**, 7847-7854.
11. N. Wang, Y. Si, N. Wang, G. Sun, M. El-Newehy, S. S. Al-Deyab and B. Ding,

Sep Purif Technol, 2014, **126**, 44-51.

12. J. P. Chen and C. H. Su, Acta Biomater, 2011, **7**, 234-243.

13. Y. Zhu, C. Gao, X. Liu and J. Shen, Biomacromolecules, 2002, **3**, 1312-1319.

14. H. S. Yoo, T. G. Kim and T. G. Park, *Adv. Drug Deliv. Rev.*, 2009, **61**, 1033-1042.

15. M. Matsusaki, H. Ajiro, T. Kida, T. Serizawa and M. Akashi, *Adv. Mater.*, 2012, **24**, 454-474.

16. L. Zhou, M. Chen, L. Tian, Y. Guan and Y. Zhang, *ACS Appl. Mater. Interfaces*, 2013, **5**, 3541-3548.

17. Y.-l. Su and C. Li, *Appl. Surf. Sci.*, 2008, **254**, 2003-2008.

18. W. J. Huang, H. J. L. Xu, Y. Xue, R. Huang, H. B. Deng and S. Y. Pan, *Food Res. Int.*, 2012, **48**, 784-791.

19. T. Zhou, Y. Huang, W. Li, Z. Cai, F. Luo, C. J. Yang and X. Chen, *Nanoscale*, 2012, **4**, 5312-5315.

20. H. Wei, Z. Wang, L. Yang, S. Tian, C. Hou and Y. Lu, *Analyst*, 2010, **135**, 1406-1410.

21. H. Cai and P. Yao, *Nanoscale*, 2013.

22. W.Y. Chen, J.Y. Lin, W.J. Chen, L. Luo, E. W.G. Diau and Y.C. Chen, *Nanomedicine*, 2010, **5**, 755-764.

23. Z. Gao and I. Zharov, *Chem. Mater.*, 2014, **26**, 2030-2037.

24. A. Shukla, J. C. Fang, S. Puranam, F. R. Jensen and P. T. Hammond, *Adv. Mater.*, 2012, **24**, 492-496.

25. I. Erel-Unal and S. A. Sukhishvili, *Macromolecules*, 2008, **41**, 3962-3970.

26. A. Mathew, P. R. Sajanlal and T. Pradeep, *J Mater. Chem.*, 2011, **21**, 11205.

27. X. Mao, B. Ding, M. Wang and Y. Yin, *Carbohydr. Polym.*, 2010, **80**, 839-844.

28. H. B. Deng, X. Zhou, X. Y. Wang, C. Y. Zhang, B. Ding, Q. H. Zhang and Y. M. Du, *Carbohydr. Polym.*, 2010, **80**, 474-479.

29. J. C. Antunes, C. L. Pereira, M. Molinos, F. Ferreira-da-Silva, M. Dessi, A. Gloria, L. Ambrosio, R. M. Goncalves and M. A. Barbosa, *Biomacromolecules*, 2011, **12**, 4183-4195.

30. Y.J. Shang, X.L. Jin, X.L. Shang, J.J. Tang, G.Y. Liu, F. Dai, Y.P. Qian, G.J. Fan, Q. Liu and B. Zhou, *Food Chem.*, 2010, **119**, 1435-1442.

31. O. Suwantong, P. Opanasopit, U. Ruktanonchai and P. Supaphol, *Polymer*, 2007, **48**, 7546-7557.

32. T. Zeng, X. Zhang, Y. Guo, H. Niu and Y. Cai, *J Mater. Chem. A*, 2014, **2**, 14807.

33. W. Li, X. Li, Q. Wang, Y. Pan, T. Wang, H. Wang, R. Song and H. Deng, *Carbohydr. Polym.*, 2014, **99**, 218-225.

34. I. Chakraborty, J. Erusappan, A. Govindarajan, K. S. Sugi, T. Udayabhaskararao, A. Ghosh and T. Pradeep, Nanoscale, 2014, 6, 8024-8031.

35. X. Cao, B. Ding, J. Yu and S. S. Al-Deyab, Carbohydr. Polym., 2012, 90, 1075-1080.

36. J. Zhao, Z. Wei, X. Feng, M. Miao, L. Sun, S. Cao, L. Shi and J. Fang, ACS Appl. Mater. Interfaces, 2014, DOI: 10.1021/am5026352.

37. B. Zhou, Y. Hu, J. Li and B. Li, Int. J Biol. Macromol., 2014, 64, 402-408.

38. D. S. Sheny, J. Mathew and D. Philip, Spectrochim. Acta. A. Mol. Biomol. Spectrosc., 2011, 79, 254-262.

39. M. Meena Kumari, S. A. Aromal and D. Philip, Spectrochim. Acta. A. Mol. Biomol. Spectrosc., 2013, 103, 130-133.

40. S. Sharma, S. Chockalingam, P. Sanpui, A. Chattopadhyay and S. S. Ghosh, Adv. Healthc. Mater., 2013, DOI: 10.1002/adhm.201300090.

41. İ. Gülçin, Z. Huyut, M. Elmastaş and H. Y. Aboul-Enein, Arabian J Chem., 2010, 3, 43-53.

42. T. J. Kim, J. L. Silva, M. K. Kim and Y. S. Jung, Food Chem., 2010, 118, 740-746.

Figure captions:

Figure 1. UV-vis spectra of Lys, Lys+OH^-, and AgNPs-Lys (A); FT-IR spectra of Lys (a), Lys+OH- (b), and AgNPs-Lys(c) (B).

Figure 2. SEM images of (a-e): cellulose nanofibrous mats, $(AgNPs\text{-}Lys/TA)_5$, $(AgNPs\text{-}Lys/TA)_{5.5}$, $(AgNPs\text{-}Lys/TA)_{10}$, and $(AgNPs\text{-}Lys/TA)_{10.5}$. Image (a'-e') showed high magnification images of a-e, respectively. The right column reveals the diameter distribution histograms of the nanofibrous mats.

Figure 3. XPS survey speatra of $(AgNPs\text{-}Lys/TA)_{10}$ (A-a) and $(AgNPs\text{-}Lys/TA)_{10.5}$ (A-b); (B-F) core-level spectra of C 1s, O 1s, N 1s, S 2p, and Ag 3d (left: $(AgNPs\text{-}Lys/TA)_{10}$, right: $(AgNPs\text{-}Lys/TA)_{10.5}$)

Figure 4. FT-IR spectra of (a-g): Lys, TA, $(AgNPs\text{-}Lys/TA)_5$, $(AgNPs\text{-}Lys/TA)_{5.5}$, $(AgNPs\text{-}Lys/TA)_{10}$, $(AgNPs\text{-}Lys/TA)_{10.5}$ and cellulose nanofibrous mats.

Figure 5. XRD patterns of TA, cellulose nanofibrous mat, $(Lys/TA)_{10}$, $(AgNPs\text{-}Lys/TA)_{10}$ (a-d).

Figure 6. Radical scavenging activities of cellulose nanofibrous mats and composite nanofibrous mats (A); plots of $\ln(C_t/C_0)$ versus reaction time for 5 bilayer, 5.5bilayer, 10bilayer, and 10.5 bilayer. C_t and C_0 are the concentrations of $DPPH^{\cdot}$ at the beginning and at time t, respectively (B).

Figure 7. Antimicrobial activities against *E. coli* and *S. aureus* of fibrous cellulose mats (control) and composite nanofibrous mats, error bars represent standard deviation (SD) for n=3.

441 Figure 1

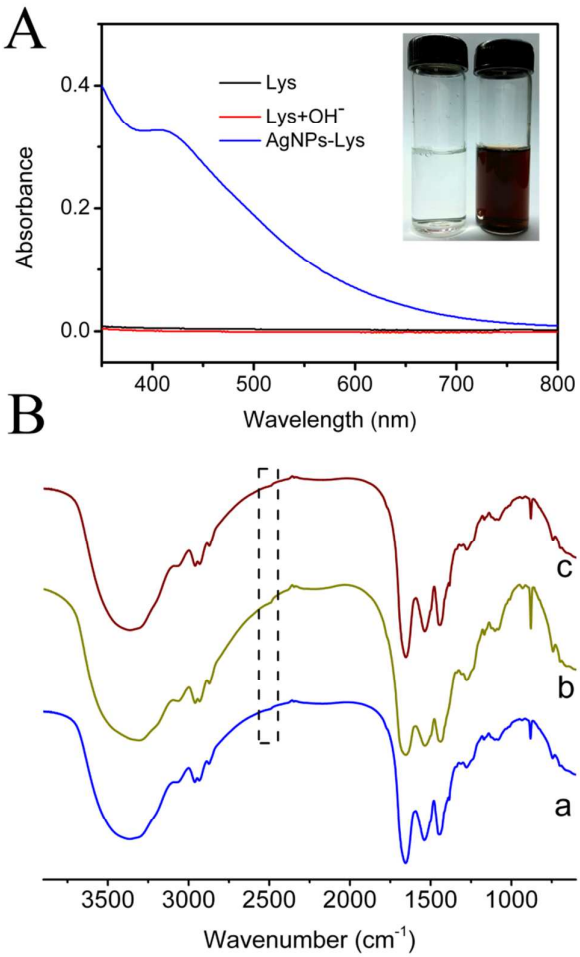

442

443

444

445

446

447

448

449

450

451

452 Figure 2

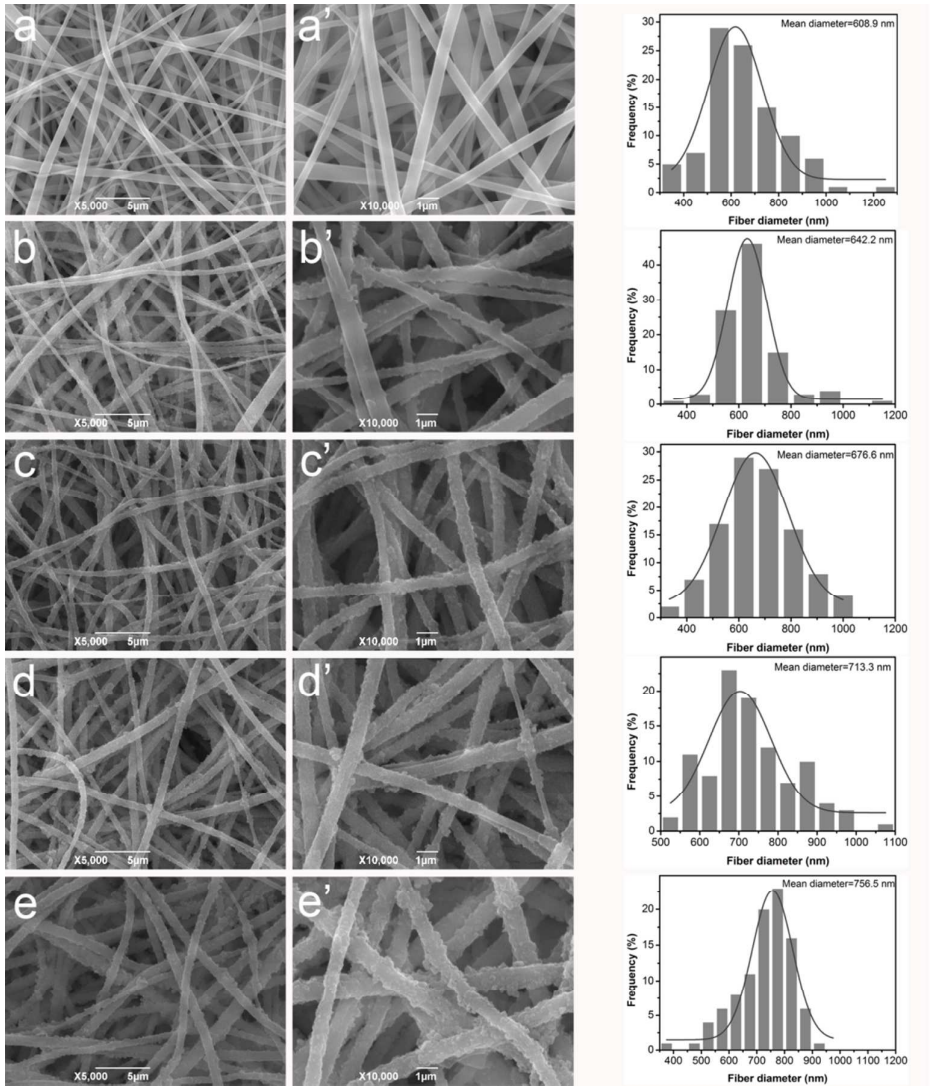

453

454

455

456

457

458

459

460

461 Figure 3

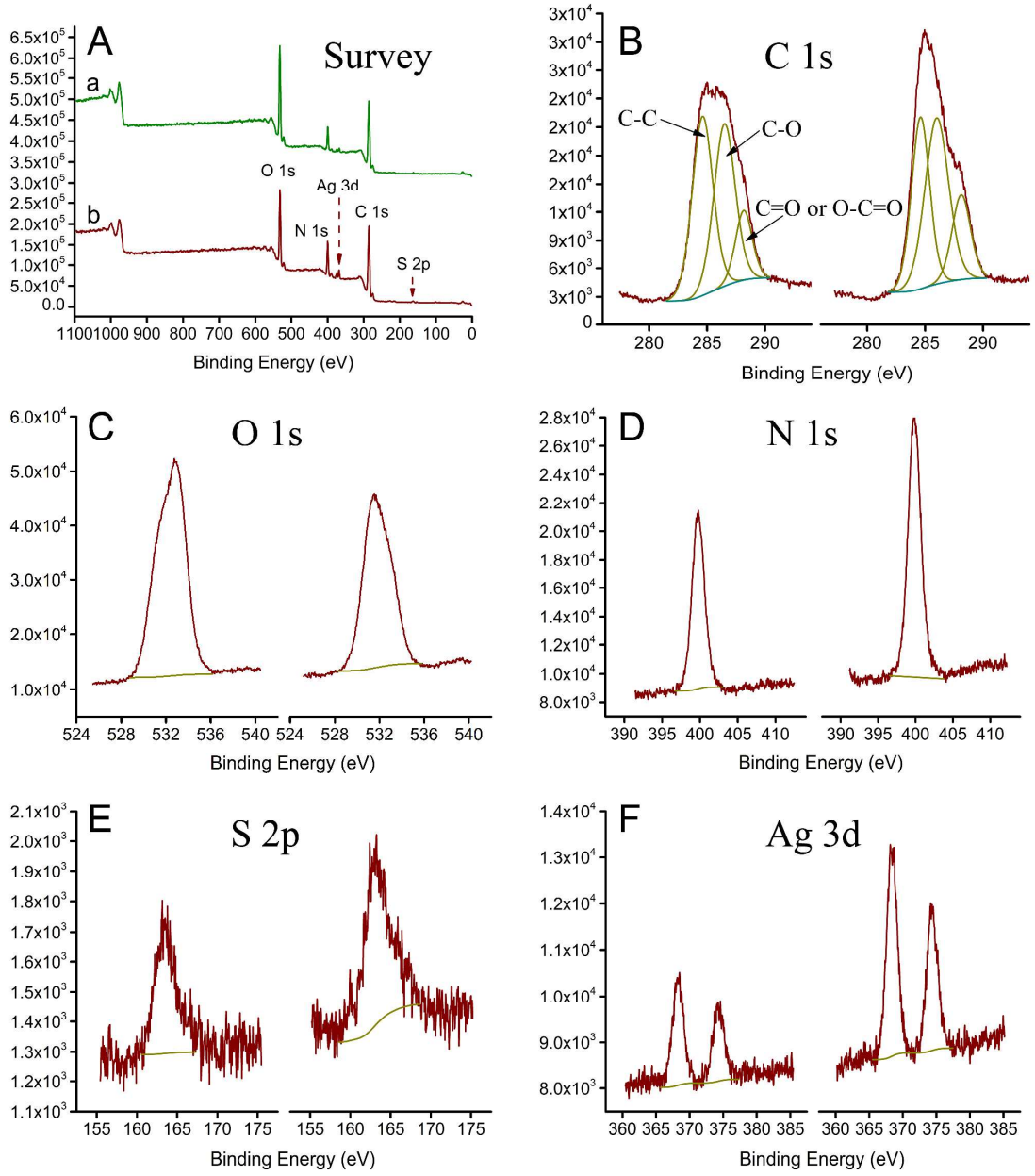

462

463

464

465

466

467

468 Figure 4

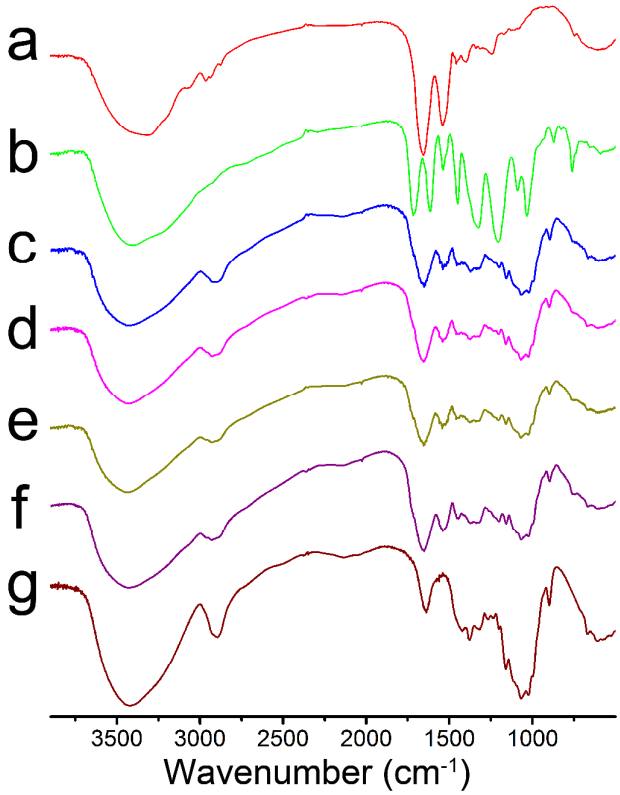

469

470

471

472

473

474

475

476

477

478

479

480

481 Figure 5

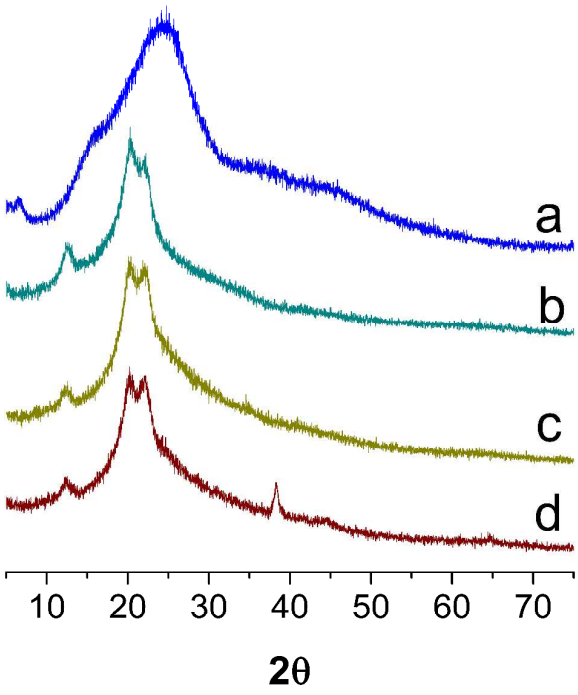

482

483

484

485

486

487

488

489

490

491

492

493

494

Figure 6

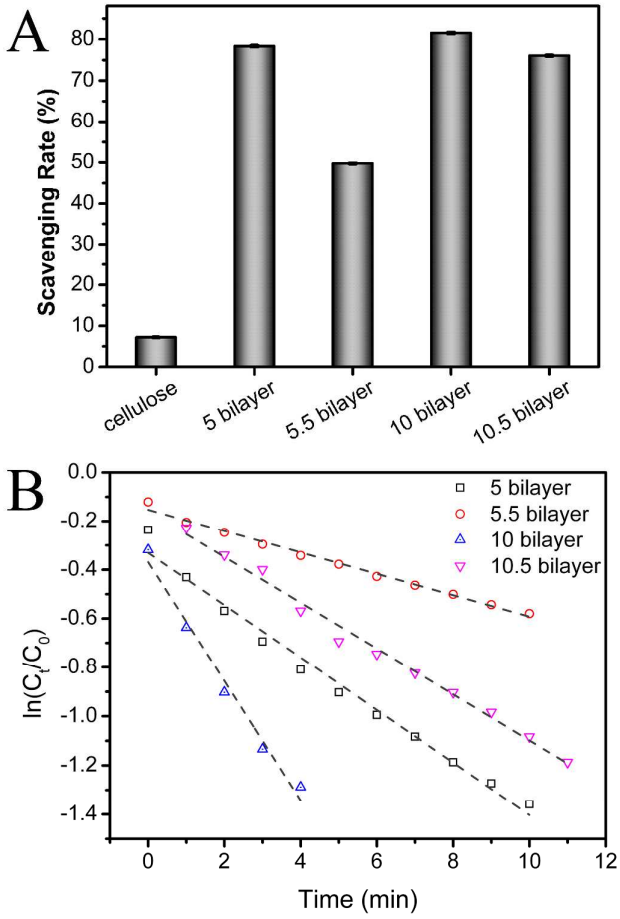

506 Figure 7

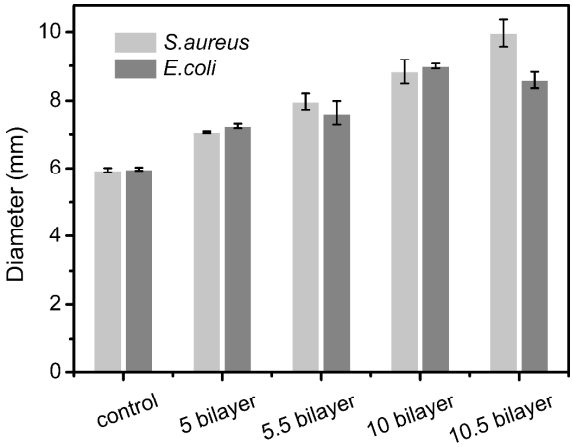

507

508

509

510

511

512

513

514

515

516

517

518

519

520

521

522

523 **Table 1**. Element composition and content on the surface of cellulose mats and

524 $(AgNPs\text{-}Lys/TA)_{10}$, and $(AgNPs\text{-}Lys/TA)_{10.5}$

Nanofibrous mats	C	O	N	S	Ag
cellulose	45.99	54.01	--	--	--
10 bilayer	62.06	27.91	9.2	0.52	0.31
10.5 bilayer	63.24	20.97	17.37	0.87	0.54

525
526
527
528
529
530
531
532
533
534